Effect of positive-energy orbitals on the photoionization cross sections and oscillator strengths of He and divalent atoms

T. N. Chang and T. K. Fang
Department of Physics and Astronomy, University of Southern California, Los Angeles, California 90089-0484
(Received 15 May 1995)

The effect of the positive-energy continuum orbitals to the photoionization and bound-bound transitions in He and Mg-like divalent Al^+ ion is estimated quantitatively in a B-spline-based configuration-interaction calculation. Our calculation has also shown that the theoretical uncertainty in radiative lifetimes measured in terms of the difference between the length and velocity results, due to the use of a parametrized long-range dipole core-polarization potential, is approximately 1–3 % for the Mg-like divalent Al^+ ion.

PACS number(s): 31.25.Jf, 32.80.Fb, 31.25.Eb, 32.70.Cs

I. INTRODUCTION

Recent applications of the B-spline-based configuration-interaction (BSCI) approach [1,2] to two-electron and divalent atoms have successfully extended the configuration-interaction (CI) basis functions beyond the products of two negative-energy one-electron bound orbitals (i.e., BB type) used in the earlier truncated diagonalization method. In particular, Chang and Wang [3] have shown that the basis function involving at least one positive-energy continuum orbital, such as a product of two continuum orbitals (i.e., CC type) or one bound and one continuum orbital (i.e., BC type), contributes significantly to the electron affinity of the ^1S ground state of H^-. Similar interactions also noticeably affect the oscillator strength for the transition from the ^1S ground state of H^- to the lowest ^1P Feshbach resonance below the $n=2$ threshold. In an eigenchannel R-matrix calculation, a similar effect in Ba photoabsorption has also been examined by Bartschat and Greene [4].

One of the purposes of this paper is to extend our BSCI study on the effect of positive-energy continuum orbitals from H^- to He and other divalent atoms. In Secs. II and III, by using initial- and final-state wave functions calculated in three different combinations of basis functions, we systematically examine the convergence of the *length* and *velocity* results of the nonresonant photoionization cross sections below the lowest doubly excited ^1P resonance and the oscillator strengths of the bound-bound transitions of the He atom. Specifically, we include in the BSCI basis (i) the BB type of functions only (i.e., a BB *calculation*), (ii) both BB and BC type of functions (i.e., a BC *calculation*), and (iii) all BB, BC, and CC type of functions (i.e., a CC *calculation*). For He nonresonant photoionization cross sections, the length-velocity difference can be as high as 5–6 % in a BC-BC calculation, which employs initial- and final-state wave functions both obtained in a BC calculation. For the oscillator strengths, the length and velocity results agree to 1–2 % or better (i.e., two to three digits) in a BC-BC calculation. Further improvement in length-velocity agreement to 0.1–0.2 % or better (i.e., three to four digits) is reached typically in a CC-CC calculation, which employs initial- and final-state wave functions both obtained in a CC calculation. In addition to the length-velocity agreement, our theoretical results are also in excellent agreement with the most accurate theoretical and experimental results.

For a divalent system, the effect due to the intrashell core excitation and intershell core-valence interactions are approximately accounted for in the BSCI calculation by a parametrized long-range core-polarization potential and a short-range model potential [2,5]. The theoretical uncertainty

TABLE I. The He $1s^2\ ^1S \rightarrow 1s\epsilon p\ ^1P$ nonresonant photoionization cross sections σ (in Mb) at selected photoelectron energy k^2 from BC-BC, CC-BC, and CC-CC calculations. The top and bottom rows represent the length and velocity results, respectively.

k^2 (eV)	BC-BC	CC-BC	CC-CC	Expt. [7]
24.578	7.435	7.345	7.403	7.40
	7.484	7.268	7.401	
25	7.233	7.165	7.219	7.21
	7.329	7.088	7.217	
27	6.341	6.373	6.412	6.40
	6.702	6.298	6.410	
29	5.641	5.681	5.707	5.70
	5.892	5.609	5.704	
31	5.035	5.071	5.085	5.10
	5.172	5.010	5.090	
33	4.526	4.557	4.563	4.57
	4.571	4.489	4.556	
35	4.069	4.099	4.097	4.09
	4.065	4.036	4.092	
37	3.667	3.696	3.689	3.68
	3.636	3.641	3.689	
39	3.320	3.348	3.336	3.32
	3.269	3.297	3.337	
41	3.016	3.043	3.027	3.01
	2.953	2.996	3.029	
43	2.751	2.777	2.759	2.72
	2.679	2.731	2.758	
45	2.519	2.544	2.523	2.48
	2.440	2.497	2.520	
47	2.312	2.335	2.313	2.28
	2.231	2.291	2.310	
49	2.129	2.151	2.128	2.10
	2.047	2.109	2.125	
51	1.967	1.988	1.963	1.94
	1.886	1.948	1.961	
53	1.824	1.844	1.819	1.77
	1.746	1.806	1.817	
55	1.701	1.720	1.694	1.67
	1.626	1.685	1.693	
57	1.603	1.620	1.594	1.61
	1.530	1.587	1.593	
59	1.598	1.611	1.582	1.56
	1.527	1.580	1.582	

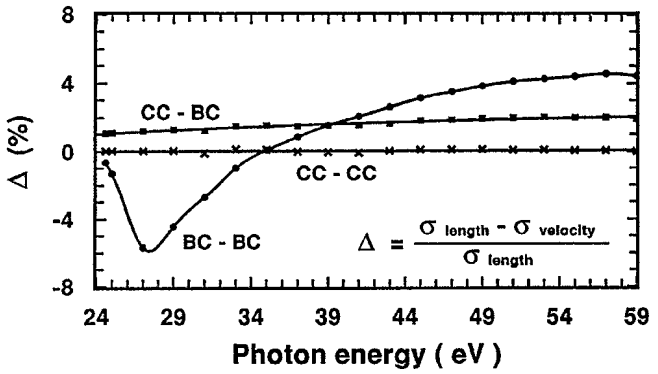

FIG. 1. Percentage difference Δ between length and velocity results for the He $1s^2\ ^1S \rightarrow 1s\epsilon p\ ^1P$ nonresonant photoionization from BC-BC, CC-BC, and CC-CC calculations.

in such a calculation is due to the combined use of the parametrized model potential and a truncated BSCI basis. Since our He calculation has already shown that the uncertainty in a CC-CC calculation for a two-electron system without an inner shell core is substantially smaller than 1%, the uncertainty in a BSCI CC-CC calculation for a divalent system can be attributed entirely to the use of the parametrized model potential. In Sec. IV, we examine in detail the variation of the length-velocity agreement in bound-bound oscillator strengths, using BB-BB, BB-BC, BC-BC, BC-CC, and CC-CC calculations for a Mg-like divalent Al^+ ion. The calculated transition probabilities for the allowed dipole transitions involving bound excited $^{1,3}S$, $^{1,3}P$, $^{1,3}D$, and $^{1,3}F$ series are also presented.

The computational procedures in a BSCI calculation for the photoionization cross sections and the oscillator strengths for the bound-bound transitions are outlined in detail elsewhere [1,2,6]. Typically, up to approximately 6000 basis functions are included in a CC calculation for a bound state. For the photoionization, a larger B-spline basis (e.g., with a total number of 120 splines or larger) is required to represent the outgoing photoelectron. The size of the BSCI basis in a CC calculation could be as large as 8000 to 9000. The diagonalization of the real symmetric Hamiltonian matrix is carried out with a modified two-step Davidson procedure [2] that can be performed with a maximum memory requirement of approximately half the size of the matrix.

II. He NONRESONANT PHOTOIONIZATION

In Table I, the cross sections σ (in Mb) at selected photoelectron energies from BC-BC, CC-BC, and CC-CC calculations for He nonresonant $1s^2\ ^1S \rightarrow 1s\epsilon p\ ^1P$ photoionization below the lowest doubly excited ^1P resonance are listed. Figure 1 summarizes the agreement between the

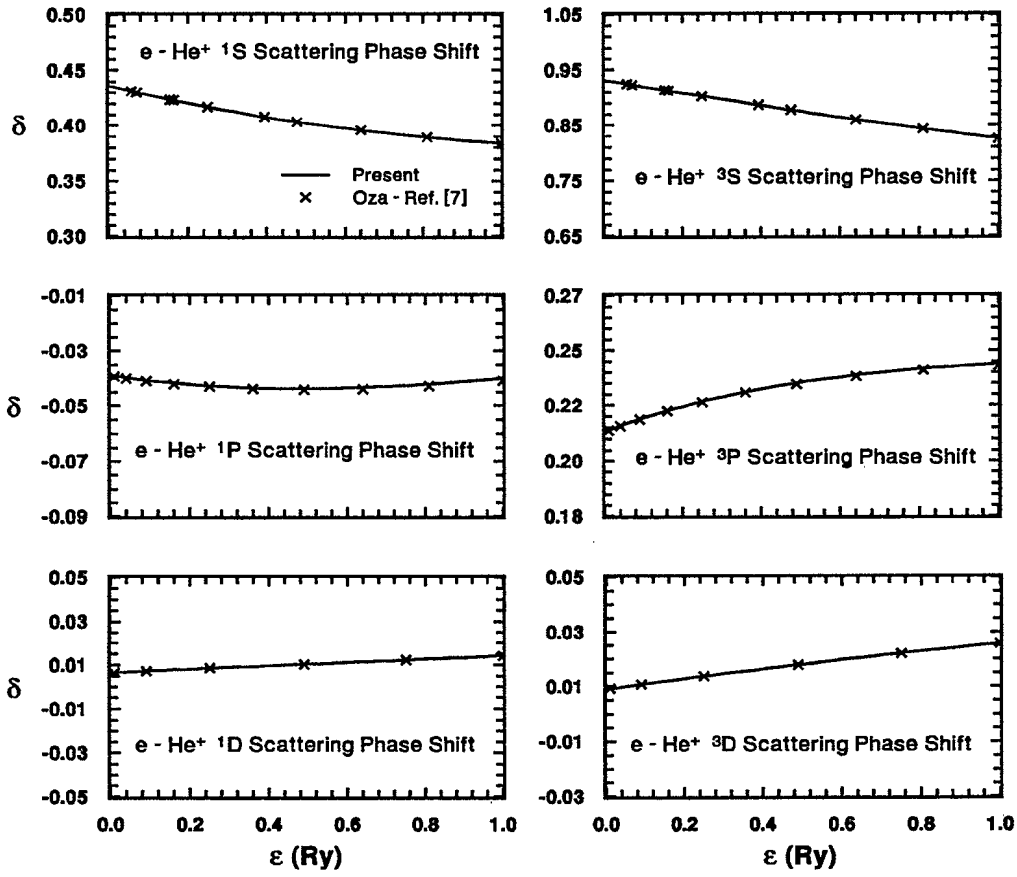

FIG. 2. Variation of nonresonant e-He^+ $^{1,3}L$ scattering phase shifts as functions of photoelectron energy ϵ.

TABLE II. The $^{1,3}S \rightarrow {}^{1,3}P$ nonresonant photoionization cross sections σ (in $a[\nu]=a\times 10^{\nu}$ Mb) from He $1sn(2,3)s\ ^{1,3}S$ states at selected wavelengths λ (in Å). The *length* and *velocity* results agree to better than 0.2%. Only *length* results are listed.

λ	$1s2s\ ^1S$	λ	$1s3s\ ^1S$	λ	$1s2s\ ^3S$	λ	$1s3s\ ^3S$
3000	8.707[+0]	6800	1.252[+1]	2500	5.289[+0]	6100	7.295[+0]
2800	7.833[+0]	6300	1.107[+1]	2300	4.859[+0]	5700	6.712[+0]
2600	6.966[+0]	5800	9.654[+0]	2150	4.505[+0]	5300	6.122[+0]
2400	6.112[+0]	5300	8.293[+0]	2000	4.127[+0]	4900	5.522[+0]
2200	5.277[+0]	4800	6.990[+0]	1850	3.731[+0]	4500	4.913[+0]
2000	4.471[+0]	4300	5.761[+0]	1700	3.321[+0]	4100	4.303[+0]
1800	3.701[+0]	3800	4.616[+0]	1550	2.902[+0]	3700	3.698[+0]
1600	2.976[+0]	3300	3.565[+0]	1400	2.480[+0]	3300	3.105[+0]
1400	2.306[+0]	2800	2.621[+0]	1250	2.064[+0]	2900	2.530[+0]
1200	1.700[+0]	2300	1.797[+0]	1100	1.661[+0]	2500	1.984[+0]
1000	1.171[+0]	1800	1.108[+0]	950	1.279[+0]	2100	1.474[+0]
800	7.247[−1]	1300	5.685[−1]	800	9.292[−1]	1700	1.014[+0]
600	3.734[−1]	900	2.576[−1]	650	6.226[−1]	1300	6.178[−1]
400	1.155[−1]	600	1.002[−1]	500	3.723[−1]	900	3.024[−1]
		400	2.957[−2]	350	2.315[−1]	500	9.172[−2]

length and velocity results. Whereas the agreement is close to 1% or better near the threshold in a BC-BC calculation , as energy increases, the velocity result is approximately 5–6 % higher than the length result at lower energy and close to 4% smaller than the length result at higher energy. The length-velocity difference is reduced substantially when the BC calculation for the initial state is replaced by a CC calculation (see the CC-BC results). The length-velocity agreement improves to approximately 0.1% in the CC-CC calculation as the calculated photoionization cross sections converge to the recently measured absolute photoabsorption cross sections by Samson *et al.* [7]. We should also note that the length results from the BC-BC calculation are within 1% of the converged cross sections from the CC-CC calculation. The quality of the continuum wave function is also illustrated by the calculated scattering phase shifts δ shown in Fig. 2. Our

TABLE III. The $^{1,3}P \rightarrow {}^{1,3}S$ nonresonant photoionization cross sections σ (in $a[\nu]=a\times 10^{\nu}$ Mb) from He $1sn(2,3)p\ ^{1,3}P$ states at selected wavelengths λ (in Å). The *length* and *velocity* results agree to better than 0.15%. Only *length* results are listed.

λ	$1s2p\ ^1P$	λ	$1s3p\ ^1P$	λ	$1s2p\ ^3P$	λ	$1s3p\ ^3P$
3500	8.575[−1]	7500	2.236[+0]	3300	9.450[−1]	7200	2.467[+0]
3250	7.207[−1]	7000	1.901[+0]	3250	9.119[−1]	7000	2.310[+0]
3000	5.965[−1]	6500	1.594[+0]	3000	7.561[−1]	6500	1.941[+0]
2750	4.847[−1]	6000	1.317[+0]	2750	6.159[−1]	6000	1.607[+0]
2500	3.853[−1]	5500	1.069[+0]	2500	4.912[−1]	5500	1.308[+0]
2250	2.982[−1]	5000	8.495[−1]	2250	3.816[−1]	5000	1.042[+0]
2000	2.231[−1]	4500	6.573[−1]	2000	2.867[−1]	4500	8.097[−1]
1750	1.600[−1]	4000	4.922[−1]	1750	2.064[−1]	4000	6.093[−1]
1500	1.083[−1]	3500	3.535[−1]	1500	1.402[−1]	3500	4.402[−1]
1250	6.797[−2]	3000	2.401[−1]	1250	8.769[−2]	3000	3.013[−1]
1000	3.833[−2]	2500	1.511[−1]	1000	4.844[−2]	2500	1.912[−1]
750	1.853[−2]	2000	8.496[−2]	750	2.173[−2]	2000	1.085[−1]
600	1.108[−2]	1500	3.993[−2]	600	1.125[−2]	1500	5.130[−2]
500	7.982[−3]	1000	1.365[−2]	450	4.507[−3]	1000	1.708[−2]
		600	3.837[−3]	360	2.000[−3]	750	7.524[−3]
						500	2.188[−3]

TABLE IV. The $^{1,3}P \rightarrow {}^{1,3}D$ nonresonant photoionization cross sections σ (in $a[\nu]=a\times 10^{\nu}$ Mb) from He $1sn(2,3)p\ ^{1,3}P$ states at selected wavelengths λ (in Å). The *length* and *velocity* results agree to better than 0.1% at longer wavelengths. At shorter wavelengths, where the cross section is a few orders of magnitude smaller, the length-velocity difference can be as high as 1%. Only *length* results are listed.

λ	$1s2p\ ^1P$	λ	$1s3p\ ^1P$	λ	$1s2p\ ^3P$	λ	$1s3p\ ^3P$
3500	1.039[+1]	7500	1.776[+1]	3300	1.316[+1]	7200	2.002[+1]
3250	8.424[+0]	7000	1.550[+1]	3250	1.269[+1]	7000	1.902[+1]
3000	6.497[+0]	6500	1.309[+1]	3000	1.027[+1]	6500	1.651[+1]
2750	4.875[+0]	6000	1.062[+1]	2750	7.981[+0]	6000	1.375[+1]
2500	3.548[+0]	5500	8.415[+0]	2500	6.045[+0]	5500	1.118[+1]
2250	2.483[+0]	5000	6.490[+0]	2250	4.436[+0]	5000	8.885[+0]
2000	1.654[+0]	4500	4.846[+0]	2000	3.129[+0]	4500	6.857[+0]
1750	1.032[+0]	4000	3.470[+0]	1750	2.100[+0]	4000	5.103[+0]
1500	5.891[−1]	3500	2.358[+0]	1500	1.319[+0]	3500	3.627[+0]
1250	2.952[−1]	3000	1.491[+0]	1250	7.572[−1]	3000	2.426[+0]
1000	1.198[−1]	2500	8.501[−1]	1000	3.814[−1]	2500	1.489[+0]
750	3.165[−2]	2000	4.164[−1]	750	1.565[−1]	2000	8.082[−1]
600	8.285[−3]	1500	1.566[−1]	600	7.825[−2]	1500	3.588[−1]
500	1.235[−3]	1000	3.387[−2]	450	3.231[−2]	1000	1.101[−1]
		600	2.453[−3]	360	1.681[−2]	750	4.657[−2]
						500	1.364[−2]

results are in excellent agreement with the 20-state close-coupling results by Oza [8]. Also, as expected, the values of δ/π at zero energy approach the observed quantum defect μ.

In Tables II–IV, we tabulate the theoretical nonresonant photoionization cross sections at selected wavelengths from a few excited $1snl\ ^{1,3}L$ states of He. The overall length-velocity agreement is approximately 0.1–0.2 %, except at shorter wavelengths where the cross sections are a few orders of magnitude smaller. Our calculated photoionization cross sections from the bound excited states are generally in agreement with the earlier close-coupling results of Jacobs

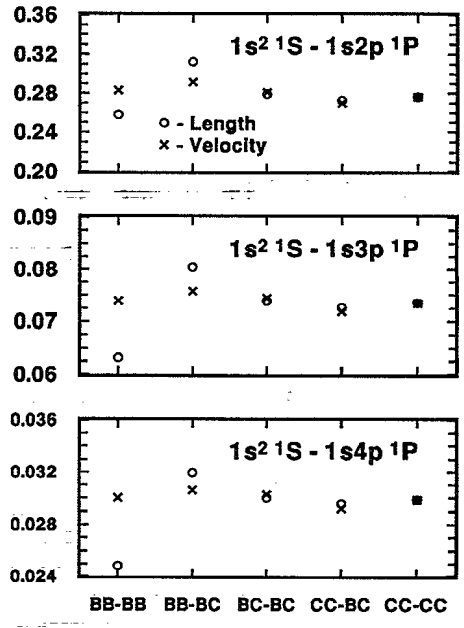

FIG. 3. Variation of theoretical oscillator strengths f for He $1s^2\ ^1S$ to $1snp\ ^1P$ transitions from BB-BB, BB-BC, BC-BC, CC-BC, and CC-CC calculations.

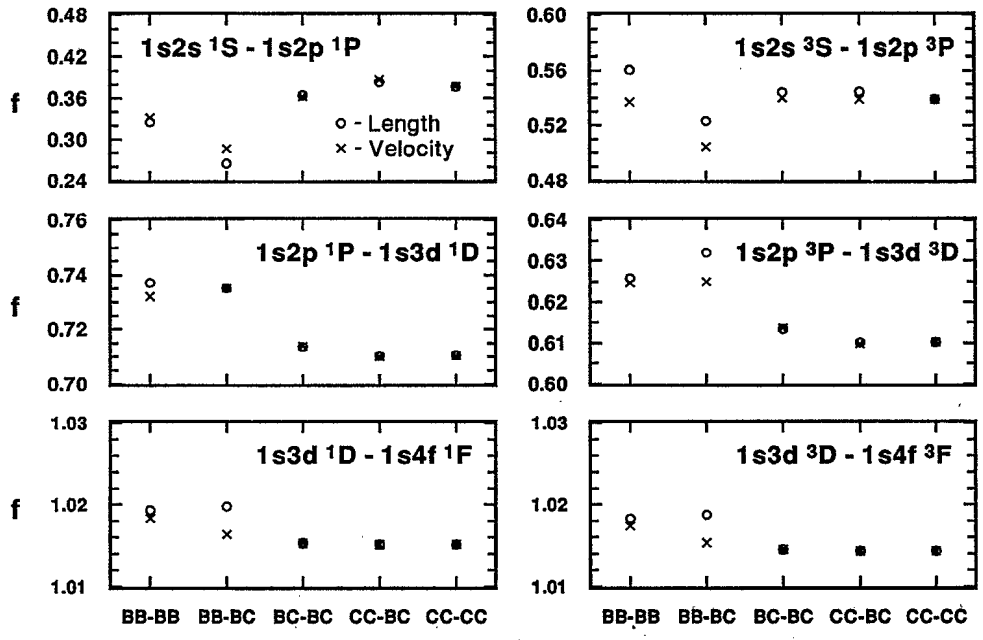

FIG. 4. Variation of theoretical oscillator strengths f for selected transitions in He from BB-BB, BB-BC, BC-BC, CC-BC, and CC-CC calculations.

[9], although the difference between the length and velocity results in the present calculation is substantially smaller. In addition to the earlier measurement by Stebbings *et al.* [10], a recent photoionization measurement from excited He atoms is now in progress, using a combined synchronized synchrotron-laser light source in a time-resolved pump-probe experiment [11].

III. He OSCILLATOR STRENGTHS

The positive-energy-orbital effect to the He $1s^2\ ^1S \rightarrow 1snp\ ^1P$ transitions is illustrated in Fig. 3 in terms of a series of calculated oscillator strengths both in length and velocity approximations from BB-BB, BB-BC, BC-BC, CC-BC, and CC-CC calculations. The large variation from BB-BB to BB-BC calculations strongly suggests a significant presence of positive-energy orbitals in the bound excited-state wave function. A less prominent but still noticeable change in the oscillator strengths between the BB-BC and BC-BC calculations suggests that the positive-energy-orbital effect is also significant for the ground state.

The positive-energy-orbital effects to the $1snl\ ^{1,3}L \rightarrow 1sm(l+1)^{1,3}(L+1)$ bound-bound transitions are illus-

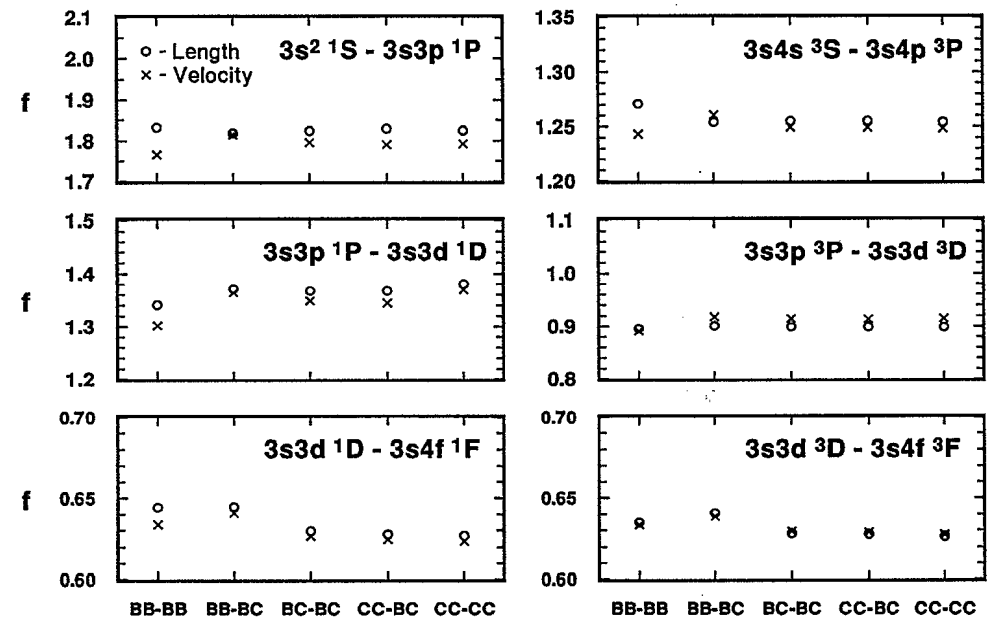

FIG. 5. Variation of theoretical oscillator strengths f for selected transitions in Mg-like Al^+ from BB-BB, BB-BC, BC-BC, CC-BC, and CC-CC calculations.

TABLE V. Calculated transition energies ΔE (in 10^3 cm^{-1}) and transition probabilities A (in 10^8 sec^{-1} or $a[\nu]=a\times10^{\nu}$ 10^8 sec^{-1}, if applicable) for allowed dipole emissions from selected $^{1,3}S$ states in Al^+. Only *length* results are listed. The theoretical transition energies are in close agreement with the observed data (not listed) in Ref. [17].

Transition	ΔE	A	Transition	ΔE	A
$3s6s\ ^1S\rightarrow3s3p\ ^1P$	72.632	0.583	$3s7s\ ^3S\rightarrow3s3p\ ^3P$	101.829	0.648
$\rightarrow3s4p\ ^1P$	25.848	0.426	$\rightarrow3s4p\ ^3P$	33.170	0.233
$\rightarrow3s5p\ ^1P$	6.913	0.305	$\rightarrow3s5p\ ^3P$	12.829	0.138
$3s5s\ ^1S\rightarrow3s3p\ ^1P$	61.194	1.307	$\rightarrow3s6p\ ^3P$	3.502	0.120
$\rightarrow3s4p\ ^1P$	14.410	1.000	$3s6s\ ^3S\rightarrow3s3p\ ^3P$	95.541	1.171
$3p^2\ ^1S\rightarrow3s3p\ ^1P$	51.755	1.051[+1]	$\rightarrow3s4p\ ^3P$	26.883	0.437
$\rightarrow3s4p\ ^1P$	4.971	0.922[−5]	$\rightarrow3s5p\ ^3P$	6.542	0.319
$3s4s\ ^1S\rightarrow3s3p\ ^1P$	35.122	3.408	$3s5s\ ^3S\rightarrow3s3p\ ^3P$	83.410	2.491
			$\rightarrow3s4p\ ^3P$	14.751	1.109
			$3s4s\ ^3S\rightarrow3s3p\ ^3P$	54.557	7.570

trated in Fig. 4. Whereas this effect remains significant for transitions involving $^{1,3}S$ and $^{1,3}P$ bound excited states, its influence on the $^{1,3}D$ and $^{1,3}F$ bound excited states appears to be somewhat smaller. In addition, our calculation suggests that a BC-BC calculation is already sufficient to generate oscillator strengths with an accuracy of approximately 1–2 % or better. Our theoretical oscillator strengths from the CC-CC calculation agree with some of the most accurate earlier theoretical results [11–13] to three to four digits. A detailed tabulation and comparison of the existing theoretical and experimental oscillator strengths were given recently by Chen [14].

IV. BOUND-BOUND TRANSITIONS IN Al^+

Similar to an earlier calculation [15], we have included a parametrized long-range core-polarization potential

$$V_\alpha(r)=-\frac{\alpha}{r^4}(1-\exp[-(r/r_0)^6]) \tag{1}$$

in the present calculation, where r_0 is a cut-off parameter and $\alpha=0.265$ a.u. is the theoretical static dipole polarizability [16]. The variations of the length-velocity difference in oscillator strength from a BB-BB to a CC-CC calculation for

TABLE VI. Calculated transition energies ΔE (in 10^3 cm^{-1}) and transition probabilities A (in 10^6 sec^{-1} or $a[\nu]=a\times10^{\nu}$ 10^6 sec^{-1}, if applicable) for allowed dipole emissions from selected $^{1,3}P$ states in Al^+. Only *length* results are listed. The theoretical transition energies are in close agreement with the observed data (not listed) from Ref. [17].

Transition	ΔE	A	Transition	ΔE	A
$3s7p\ ^1P\ \rightarrow3s^2\ ^1S$	140.292	6.269	$3s4p\ ^1P\ \rightarrow3s^2\ ^1S$	107.303	5.079
$\rightarrow3s4s\ ^1S$	44.652	3.027[+1]	$\rightarrow3s4s\ ^1S$	11.663	3.111[+1]
$\rightarrow3p^2\ ^1S$	28.018	0.811	$\rightarrow3p^2\ ^1D$	22.284	6.307[+1]
$\rightarrow3s5s\ ^1S$	18.579	1.434	$3s3p\ ^1P\ \rightarrow3s^2\ ^1S$	60.519	1.486[+3]
$\rightarrow3s6s\ ^1S$	7.141	0.213	$3s7p\ ^3P\ \rightarrow3s4s\ ^3S$	48.854	2.514
$\rightarrow3p^2\ ^1D$	55.273	4.029[+1]	$\rightarrow3s5s\ ^3S$	20.001	0.230[−3]
$\rightarrow3s3d\ ^1D$	29.649	1.042[+1]	$\rightarrow3s6s\ ^3S$	7.870	0.132
$\rightarrow3s4d\ ^1D$	14.981	2.203	$\rightarrow3s7s\ ^3S$	1.582	1.432
$\rightarrow3s5d\ ^1D$	5.955	0.436	$\rightarrow3s3d\ ^3D$	44.633	0.102
$\rightarrow3s6d\ ^1D$	0.609	0.157	$\rightarrow3s4d\ ^3D$	18.624	0.484
$3s6p\ ^1P\ \rightarrow3s^2\ ^1S$	135.290	5.984	$\rightarrow3s5d\ ^3D$	7.269	0.399
$\rightarrow3s4s\ ^1S$	39.650	1.942[+1]	$\rightarrow3s6d\ ^3D$	1.271	1.156
$\rightarrow3p^2\ ^1S$	23.016	0.485	$3s6p\ ^3P\ \rightarrow3s4s\ ^3S$	43.770	0.960
$\rightarrow3s5s\ ^1S$	13.578	0.480	$\rightarrow3s5s\ ^3S$	14.917	0.231
$\rightarrow3s6s\ ^1S$	2.139	1.850	$\rightarrow3s6s\ ^3S$	2.785	3.744
$\rightarrow3p^2\ ^1D$	50.271	4.053[+1]	$\rightarrow3s3d\ ^3D$	39.549	0.514
$\rightarrow3s3d\ ^1D$	24.647	1.157[+1]	$\rightarrow3s4d\ ^3D$	13.540	1.026
$\rightarrow3s4d\ ^1D$	9.979	2.015	$\rightarrow3s5d\ ^3D$	2.185	2.573
$\rightarrow3s5d\ ^1D$	0.954	0.275	$3s5p\ ^3P\ \rightarrow3s4s\ ^3S$	34.442	1.143[−2]
$3s5p\ ^1P\ \rightarrow3s^2\ ^1S$	126.237	3.304	$\rightarrow3s5s\ ^3S$	5.590	1.210[+1]
$\rightarrow3s4s\ ^1S$	30.597	7.414	$\rightarrow3s3d\ ^3D$	30.222	1.866
$\rightarrow3p^2\ ^1S$	13.963	0.215	$\rightarrow3s4d\ ^3D$	4.213	6.313
$\rightarrow3s5s\ ^1S$	4.525	6.855	$3s4p\ ^3P\ \rightarrow3s4d\ ^3S$	14.101	5.545[+1]
$\rightarrow3p^2\ ^1D$	41.218	4.602[+1]	$\rightarrow3s3d\ ^3D$	9.881	1.581[+1]
$\rightarrow3s3d\ ^1D$	15.594	1.526[+1]			
$\rightarrow3s4d\ ^1D$	0.927	0.949[−1]			

TABLE VII. Calculated transition energies ΔE (in 10^3 cm^{-1}) and transition probabilities A (in 10^7 sec^{-1} or $a[v]=a\times10^v$ 10^7 sec^{-1}, if applicable) for allowed dipole emissions from selected $^{1,3}D$ states in Al^+. Only *length* results are listed. The theoretical transition energies are in close agreement with the observed data (not listed) from Ref. [17].

Transition	ΔE	A	Transition	ΔE	A
$3s6d\ ^1D \rightarrow 3s3p\ ^1P$	79.164	1.017[+1]	$3d7d\ ^3D \rightarrow 3d3p\ ^3P$	105.693	0.869
$\rightarrow 3s4p\ ^1P$	32.380	1.077	$\rightarrow 3s4p\ ^3P$	37.035	0.277
$\rightarrow 3s5p\ ^1P$	13.445	1.161	$\rightarrow 3s5p^3P$	16.694	0.383
$\rightarrow 3s6p\ ^1P$	4.393	0.921	$\rightarrow 3s6p\ ^3P$	7.367	0.342
$\rightarrow 3s4f\ ^1F$	15.861	0.216[−1]	$\rightarrow 3s7p\ ^3P$	2.283	0.380
$\rightarrow 3s5f\ ^1F$	5.637	0.569[−1]	$\rightarrow 3s4f\ ^3F$	19.005	0.449[−1]
$\rightarrow 3s6f\ ^1F$	0.064	0.155[−4]	$\rightarrow 3s5f\ ^3F$	9.017	0.486[−1]
$3s5d\ ^1D \rightarrow 3s3p\ ^1P$	73.818	2.373[+1]	$\rightarrow 3s6f\ ^3F$	4.036	0.503[−2]
$\rightarrow 3s4p\ ^1P$	27.034	3.230	$\rightarrow 3p3d\ ^3F$	1.443	0.816[−1]
$\rightarrow 3s5p\ ^1P$	8.099	2.646	$3s6d\ ^3D \rightarrow 3s3p\ ^3P$	102.140	1.758
$\rightarrow 3s4f\ ^1F$	10.515	0.387[−1]	$\rightarrow 3s4p\ ^3P$	33.481	0.728
$\rightarrow 3s5f\ ^1F$	0.291	0.559[−3]	$\rightarrow 3s5p\ ^3P$	13.140	0.851
$3s4d\ ^1D \rightarrow 3s3p\ ^1P$	64.792	6.704[+1]	$\rightarrow 3s6p\ ^3P$	3.813	0.935
$\rightarrow 3s4p\ ^1P$	18.008	9.263	$\rightarrow 3s4f\ ^3F$	15.451	0.914[−1]
$\rightarrow 3s4f\ ^1F$	1.489	0.179[−1]	$\rightarrow 3s5f\ ^3F$	5.463	0.109
$3s3d\ ^1D \rightarrow 3s3p\ ^1P$	50.125	1.388[+2]	$\rightarrow 3s6f\ ^3F$	0.482	0.381[−2]
$\rightarrow 3s4p\ ^1P$	3.340	0.674[−1]	$3s5d\ ^3D \rightarrow 3s3p\ ^3P$	96.142	4.363
$3p^2\ ^1D \rightarrow 3s3p\ ^1P$	24.500	0.398[−1]	$\rightarrow 3s4p\ ^3P$	27.483	2.308
			$\rightarrow 3s5p\ ^3P$	7.142	2.809
			$\rightarrow 3s4f\ ^3F$	9.453	0.232
			$3s4d\ ^3D \rightarrow 3s3p\ ^3P$	84.787	1.550[+1]
			$\rightarrow 3s4p\ ^3P$	16.128	1.147[+1]
			$3s3d\ ^3D \rightarrow 3s3p\ ^3P$	58.778	1.243[+2]

selected bound-bound transitions in the Al^+ ion are shown in Fig. 5. For most of the transitions, the length-velocity agreement improves from a BB-BB calculation to a BC-BC calculation, suggesting that the positive-energy-orbital effect remains significant for a divalent system. Unlike in He atom, the length-velocity agreements in oscillator strengths for the Al^+ ion are not improved significantly from a BC-BC calculation to a CC-CC calculation. This can be attributed directly to the use of parametrized model potential. For transitions with an oscillator strength greater than 0.01, the length-velocity agreement generally stays at a level of approximately 1–2 % or better. In contrast, the length-velocity difference for a transition with an oscillator strength significantly smaller than 0.01 could easily exceed 10%. For transitions involving $3s^2\ ^1S$ and $3p^2\ ^1S$ states, the length-velocity differences are relatively large, suggesting also that the parametrized model potential is inadequate to account for the intrashell core excitation and intershell core-valence in-

TABLE VIII. Calculated transition energies ΔE (in 10^3 cm^{-1}) and transition probabilities A (in 10^7 sec^{-1} or $a[v]=a\times10^v$ 10^7 sec^{-1}, if applicable) for allowed dipole emissions from selected $^{1,3}F$ states in Al^+. Only *length* results are listed. The theoretical transition energies are in close agreement with the observed data (not listed) from Ref. [17].

Transition	ΔE	A	Transition	ΔE	A
$3s7f\ ^1F \rightarrow 3p^2\ ^1D$	57.964	5.734	$3s7f\ ^3F \rightarrow 3s3d\ ^3D$	47.789	1.699[+1]
$\rightarrow 3s3d\ ^1D$	32.340	0.902	$\rightarrow 3s4d\ ^3D$	21.780	1.099
$\rightarrow 3s4d\ ^1D$	17.672	0.343	$\rightarrow 3s5d\ ^3D$	10.425	0.241
$\rightarrow 3s5d\ ^1D$	8.646	0.620	$\rightarrow 3s6d\ ^3D$	4.427	0.339[−1]
$\rightarrow 336d\ ^1D$	3.300	0.460	$\rightarrow 3s7d\ ^3D$	0.873	0.559[−1]
$3s6f\ ^1F \rightarrow 3p^2\ ^1D$	54.599	8.677	$3p3d\ ^3F \rightarrow 3s3d\ ^3D$	45.473	2.638[+1]
$\rightarrow 3s3d\ ^1D$	28.975	0.578	$\rightarrow 3s4d\ ^3D$	19.464	0.254
$\rightarrow 3s4d\ ^1D$	14.308	0.990	$\rightarrow 3s5d\ ^3D$	8.109	0.111[−1]
$\rightarrow 3s5d\ ^1D$	5.282	1.228	$\rightarrow 3s6d\ ^3D$	2.111	0.264
$3s5f\ ^1F \rightarrow 3p^2\ ^1D$	49.027	1.409[+1]	$3s6f\ ^3F \rightarrow 3s3d\ ^3D$	42.880	5.410
$\rightarrow 3s3d\ ^1D$	23.403	0.270[−1]	$\rightarrow 3s4d\ ^3D$	16.871	1.035
$\rightarrow 3s4d\ ^1D$	8.735	3.414	$\rightarrow 3s5d\ ^3D$	5.516	1.145
$3s4f\ ^1F \rightarrow 3p^2\ ^1D$	38.803	2.476[+1]	$3s5f\ ^3F \rightarrow 3s3d\ ^3D$	37.899	2.465
$\rightarrow 3s4d\ ^1D$	13.178	5.187	$\rightarrow 3s4d\ ^3D$	11.890	4.196
			$\rightarrow 3s5d\ ^3D$	0.535	0.249[−2]
			$3s4f\ ^3F \rightarrow 3s3d\ ^3D$	27.911	2.325[+1]
			$\rightarrow 3s4d\ ^3D$	1.902	0.351[−1]

TABLE IX. The radiative lifetimes τ (in 10^{-8} sec) for selected excited states of Al^+.

State	τ_{length}	$\tau_{velocity}$	State	τ_{length}	$\tau_{velocity}$
$3s4s\ ^1S$	0.293	0.298	$3s4s\ ^3S$	0.132	0.134
$3p^2\ ^1S$	0.095	0.094	$3s5s\ ^3S$	0.278	0.281
$3s5s\ ^1S$	0.433	0.439	$3s6s\ ^3S$	0.519	0.525
$3s6s\ ^1S$	0.761	0.771	$3s7s\ ^3S$	0.878	0.888
$3s3p\ ^1P$	0.067	0.068	$3s4p\ ^3P$	1.403	1.396
$3s4p\ ^1P$	1.007	1.000	$3s5p\ ^3P$	4.928	4.853
$3s5p\ ^1P$	1.263	1.244	$3s6p\ ^3P$	11.052	10.827
$3s6p\ ^1P$	1.211	1.203	$3s7p\ ^3P$	16.079	15.843
$3s7p\ ^1P$	1.081	1.083			
$3p^2\ ^1D$	251.26	833.33	$3s3d\ ^3D$	0.080	0.079
$3s3d\ ^1D$	0.072	0.073	$3s4d\ ^3D$	0.371	0.361
$3s4d\ ^1D$	0.131	0.131	$3s5d\ ^3D$	1.030	0.995
$3s5d\ ^1D$	0.337	0.333	$3s6d\ ^3D$	2.234	2.151
$3s6d\ ^1D$	0.746	0.732	$3s7d\ ^3D$	4.113	3.953

teractions for states that are dominated by strong mixing between $3s^2$ and $3p^2$ configurations.

Instead of a detailed tabulation of the oscillator strengths, we have listed in Tables V–VIII the transition probabilities A_{fi} and the transition energies ΔE_{fi} of selected bound-bound transitions from an upper state $|f\rangle$ to a lower state $|i\rangle$. The calculated transition energies are in close agreement with the observed data (not listed) from Ref. [17]. The transition probability A_{fi}, given in units of ns^{-1} (i.e., 10^9 sec^{-1}), is related to the transition energy ΔE_{fi} in Ry units and the oscillatory strength f^e_{if} for an *emission* from $|f\rangle$ to $|i\rangle$ by [18]

$$A_{fi}=8.0323(\Delta E_{fi})^2|f^e_{if}|. \tag{2}$$

The radiative lifetime τ_f of an excited state $|f\rangle$ can be evaluated readily from the sum of the listed transition probabilities A_{fi} for all allowed emissions from state $|f\rangle$ to lower states $|i\rangle$. Table IX summarizes the radiative lifetimes derived from the transition probabilities tabulated in Tables V–VIII. They are in general slightly smaller than the ones from our earlier limited BC-BC calculation [15]. Except for the long-lived $3p^2\ ^1D$ state, our calculated length and velocity results generally agree to 1–3 % or better. For the $3p^2\ ^1D$ state, the radiative lifetimes in length and velocity approximations are 1.97×10^{-6} sec and 8.27×10^{-6} sec, respectively, from our earlier BC-BC calculation [15]. In the present CC-CC calculation, this difference remains large although it has improved slightly over the earlier results. A summary of other earlier observed and calculated data is given in [15].

ACKNOWLEDGMENT

This work was supported by NSF under Grant No. PHY94-13338.

[1] T. N. Chang and X. Tang, Phys. Rev. A **44**, 232 (1991).
[2] T. N. Chang, in *Many-body Theory of Atomic Structure and Photoionization*, edited by T. N. Chang (World Scientific, Singapore, 1993), p. 213.
[3] T. N. Chang and R. Q. Wang, Phys. Rev. A **43**, 1218 (1991).
[4] K. Bartschat and C. H. Greene, J. Phys. B **26**, L109 (1993).
[5] T. N. Chang and K. T. Chung, Chin. J. Phys. **27**, 425 (1989).
[6] T. N. Chang, Phys. Rev. A **36**, 447 (1987).
[7] J. A. R. Samson, Z. X. He, L. Yin, and G. N. Haddad, J. Phys. B **27**, 887 (1994).
[8] D. H. Oza, Phys. Rev. A **33**, 824 (1986).
[9] V. L. Jacobs, Phys. Rev. A **3**, 289 (1971); **9**, 1938 (1974).
[10] R. F. Stebbings, F. B. Dunning, F. K. Tittel, and R. D. Rundel, Phys. Rev. Lett. **30**, 815 (1973).
[11] J. Lacoursiere, M. Meyer, L. Nahon, P. Morin, and M. Larzilliere, Nucl. Instrum. Methods Phys. Res. A **351**, 545 (1994).
[12] B. Schiff, C. L. Pekeris, and Y. Accad, Phys. Rev. A **4**, 885 (1971).
[13] A. Kono and S. Hattori, Phys. Rev. A **29**, 2981 (1984).
[14] M. K. Chen, J. Phys. B **27**, 4847 (1994); **27**, 865 (1994).
[15] T. N. Chang and R. W. Wang, Phys. Rev. A **44**, 80 (1991).
[16] G. A. Victor, R. F. Stewart, and C. Laughlin, Astrophys. J. Suppl. Ser. **31**, 237 (1976).
[17] W. C. Martin and R. Zalubas, J. Phys. Chem. Ref. Data **8**, 817 (1979).
[18] T. N. Chang, Phys. Rev. A **41**, 4922 (1990).